Metalloporphyrin Gas and Condensed-Phase Resonance Raman Studies: The Role of Vibrational Anharmonicities as Determinants of Raman Frequencies

Sanford A. Asher* and James Murtaugh

Contribution from the Department of Chemistry, University of Pittsburgh, Pittsburgh, Pennsylvania 15260. *Received May 23, 1983*

Abstract: The first resonance Raman spectra of gas-phase porphyrins are reported. An extensive temperature-dependent study of the Raman spectra of nickel(II) and cobalt(II) octaethylporphine both in the gas phase and in condensed solution phases demonstrates a large temperature dependence of the Raman frequencies. The small frequency differences observed between the gas- and condensed-phase samples indicate that the van der Waals interactions occurring in hydrocarbon solvents do not affect the heme frequencies. The temperature dependence of the Raman frequencies shows an apparent activation energy. This temperature dependence is interpreted as arising from anharmonic interactions between high-frequency vibrations and thermally populated low-frequency vibrations. Frequency shifts as large as 15 cm^{-1} are observed between 40 and 600 K for the heme core size dependent Raman vibrations. These shifts may be interpreted as an expansion of the heme ring as low-frequency vibrations are thermally populated. The large temperature dependence of the heme vibrational frequencies may account for some of the spectral shifts observed in photochemically generated transient Raman studies in heme proteins. Transient heme temperature increases of greater than 100 K are expected to occur during photolysis of liganded heme complexes such as carbon monoxyhemoglobin and carbon monoxymyoglobin. This temperature increase will result in shifts to lower frequency for the heme Raman vibrations.

Resonance Raman spectroscopy is a relatively recent addition to the vast array of spectroscopic techniques used to determine bonding, structure, and intermolecular interactions in liquid and solid samples.[1] A major advantage of resonance Raman spectroscopy is its selectivity for individual chromaphoric species in a multicomponent sample or within a macromolecule. This selectivity has been extensively utilized for biophysical studies of a variety of proteins, nucleic acids, visual pigments, etc., in both in vivo and in vitro systems.[2-4]

All of these studies interpret the observed resonance Raman vibrational frequencies in terms of specific bonding, geometries, and intermolecular interactions. Generally these interpretations rely upon previous studies of model compounds that were designed to mimic the structure of the molecular species thought to exist in the more complicated sample. Recently a series of time-resolved transient Raman techniques has evolved to study transient molecular species that exist in the picosecond and nanosecond time regimes.[5-10] The structural interpretations of the Raman spectra of these transient species similarly depend upon model compound data.

In this study we have examined for the first time the resonance Raman spectra of heme model compounds, such as nickel octaethylporphine (NiOEP) and cobalt octaethylporphine (CoOEP), in both the gas phase and the condensed phase. These studies calibrate the effect of nonspecific van der Waals interactions on metalloporphyrin structure as reported by the Raman molecular vibrational frequencies. We also examine the temperature dependence of the resonance Raman spectra in both the gaseous and condensed phases. These studies indicate that anharmonic coupling between molecular vibrations is important in determining Raman frequencies.

Raman frequency shifts can derive from changes in anharmonic coupling between molecular vibrations. Thus, caution must be exercised when interpreting small frequency shifts in terms of structural changes. For example, it is generally assumed that the frequency shift in a vibration mode ν_a derives from a change in bonding or geometry for those nuclei undergoing harmonic displacements. However, this study indicates that frequency shifts for ν_a in a metalloporphyrin could also derive from changes in anharmonic coupling between the vibrational mode under study, ν_a, and other vibrational modes in the molecule. The coupling vibrational mode, ν_b, may possess atomic displacement contributions not present to a major extent in ν_a. A change in bonding or structure for nuclei in ν_b could be communicated as a frequency shift for ν_a. Thus, a frequency shift in ν_a may be observed even in the absence of any changes in bonding or geometry for nuclei directly involved in mode ν_a.

This study indicates the importance of the anharmonic coupling between low-frequency porphyrin vibrational modes and the structure-sensitive heme Raman vibrations by demonstrating the existence of a large temperature dependence for the porphyrin vibrational frequencies. Temperature-dependent frequency shifts have previously been observed for the Fe-proximal histidine bond in deoxyhemoglobin (Hb).[11] The temperature-dependent frequency shifts indicate that care must be exercised when interpreting the frequency shifts observed in transient Raman studies of heme proteins if the transient species is photochemically generated. For example, if the effective temperature of the generated transient species is greater than that of the thermally equilibrated species, frequency shifts of the Raman peaks will occur which are unrelated to any changes in molecular bonding and structure between the transient and equilibrium moieties. The work reported here also supports recent theoretical models of molecular relaxation which propose that dephasing and relaxation of high-frequency vibrations occur through an anharmonic coupling with low-frequency modes that exchange energy with the environment.[12-14]

(1) Clark, R. J. H.; Stewart B. *Struct. Bonding (Berlin)* **1979**, *36*, 1.
(2) Asher, S. A. *Methods Enzymol.* **1981**, *76*, 371.
(3) Carey, P. R. "Biochemical Applications of Raman and Resonance Raman Spectroscopies"; Academic Press: New York, 1982.
(4) Tu, A. T. "Raman Spectroscopy in Biology: Principles and Applications"; Wiley: New York, 1982.
(5) Friedman, J. M.; Rousseau, D. L.; Ondrias, M. R. *Annu. Rev. Phys. Chem.* **1982**, *33*, 471.
(6) Friedman, J. M.; Lyons, K. B. *Nature (London)* **1980**, *284*, 570.
(7) Terner, J.; Strong, J. D.; Spiro, T. G.; Nagumo, M.; Nicol, M.; El-Sayed, M. A. *Proc. Natl. Acad. Sci. U.S.A.* **1981** *78*, 1313.
(8) Stein, P.; Terner, J.; Spiro, T. G. *J. Phys. Chem.* **1982**, *86*, 168.
(9) Irwin, M. J.; Atkinson, G. H. *Nature (London)* **1981**, *293*, 317.
(10) Terner, J.; Voss, D. F.; Paddock, C.; Miles, R. B.; Spiro, T. G. *J. Phys. Chem.* **1982**, *86*, 859.
(11) Ondrias, M. R.; Rousseau, D. L.; Simon, S. R. *Proc. Natl. Acad. Sci. U.S.A.* **1982**, *79*, 1511.
(12) Harris, C. B.; Shelby, R. M.; Cornelius, P. A. *Phys. Rev. Lett.* **1977**, *38*, 1415.
(13) Shelby, R. M.; Harris, C. B.; Cornelius, P. A. *J. Chem. Phys.* **1979**, *70*, 34.

0002-7863/83/1505-7244$01.50/0

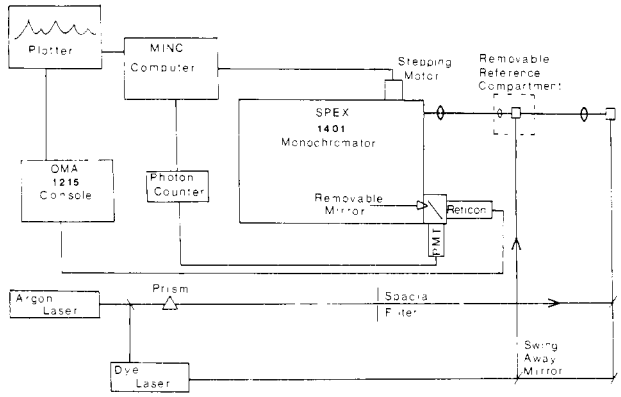

Figure 1. Block diagram of a Raman spectrometer showing sample and reference compartments.

Experimental Section

Octaethylporphin (OEP) was obtained from Porphyrin Products Inc. and from Strem Chemical Co. The OEP from Strem was recrystallized from benzene before use. High-purity $Co(OAc)_2$ was obtained from Spex Industries. Reagent Grade $NiCl_2$ was obtained from J. T. Baker Co. Dow Corning 705 silicone diffusion pump oil was used as the high-temperature solvent.

Preparation of Materials. CoOEP: The synthesis procedure used was similar to that of Adler et al.[15] and Bonnett and Dimsdale.[16] OEP (0.0463 g) was added by soxhlet extraction to a solution of 2 mL of acetic anhydride, 13 mL of acetic acid, and 0.0611 g of $Co(CH_3CO_2)_2$ under a nitrogen flow. Absorption spectral measurements monitored completion of the reaction. The absorption spectra agreed with previously reported data.[16] The small red crystals obtained were filtered, dissolved in 46 °C benzene, and refiltered. Cooling the solution over a period of 3 days from 46 °C to room temperature yielded long red needle-like crystals 1 cm in length. The above procedure removed fluorescent impurities with emission spectral maxima at 535 and 580 nm. We were unable remove these impurities by chromatography with alumina (neutral and basic), or silica gel. We typically observe severe band broadening and/or porphyrin degradation with the use of previously published chromatographic techniques.[16-18] Our inability to chromatographically purify CoOEP and NiOEP using previously published procedures is consistent with more recent reports.[19-21]

NiOEP: NiOEP was synthesized by using techniques similar to those for CoOEP. $NiCl_2$ (0.3634 g) was dissolved in a mixture of 60 mL of acetic acid and 10 mL of acetic anhydride. OEP (0.1147 g) was added to this solution by soxhlet extraction, and after ca. 12 h, the crystals were filtered and dissolved in 47 mL of boiling benzene. The filtered hot solution was recrystallized as previously described. The absorption spectra agreed with previously reported data.[22]

Instrumentation. The gas-phase absorption measurements were obtained by using a 1.5 cm path length cell placed in a temperature-controlled oven built for this study. The absorption spectra were measured by using a Cary 14 absorption spectrophotometer.

The Raman spectra were excited by using a Spectraphysics Model 164 Ar ion laser and a Spectraphysics Model 375B jet stream dye laser (Figure 1). The scattered light was dispersed by using a modified Spex 1401 monochromator. A stepping motor attached to the Spex 1401 was interfaced to a Digital Equipment Corporation Minc-11 computer which was used for repetitively scanning the spectra and displaying the data. The scattered light was detected by using conventional photon counting equipment or a Reticon multichannel array. The computer interfaced photon counting system included a PAR 1121 amplifer–discriminator, a PAR 1109 photon counter, and a cooled RCA C31034A-02 photomultiplier. The multichannel array consisted of a PAR OMA II system

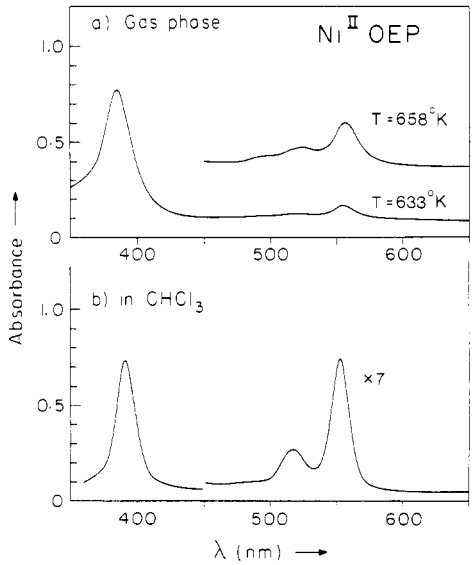

Figure 2. Absorption spectrum of nickel(II) octaethylporphine: (a) in the gas phase at 658 and 633 K, path length = 1.5 cm; (b) in $CHCl_3$ solution at room temperature, path length = 1.0 cm, concentration ≃ 2.6×10^{-6} M.

that included a Model 1420 intensified Reticon detector, a 1218 controller, and a PAR 1215 computer acquisition system.

The Spex 1401 monochromator was modified to support both a PMT and a Reticon detector by replacing the middle slit with a new slit assembly that consisted of a keyed holder which accepted a series of fixed slits. The final mirror in the Spex 1401 was replaced with a longer 1 m focal length mirror. An assembly that contained the Reticon detector and a slit photomultiplier assembly was mounted on the outside of the monochromator exit port. When the photon-counting system was used, a removable 45° mirror deflected the dispersed scattered light through a slit to the PMT.

The NiOEP resonance Raman measurements obtained by using the Reticon detector were calibrated before and after each measurement by using indene as a frequency standard. No scanning of the monochromator occurred between measurements or calibrations. Furthermore the calibration was obtained without any movement of the sample. The reference and sample chambers contained their own separate collection optics. A removable 45° mirror was used to redirect the laser from the sample chamber to a position between the sample collection optics and the Spex 1401 entrance slit. The indene reference capillary and its collection optics were lowered into position to obtain the spectrum of indene. The standard deviation of frequency measurements for the indene reference using an Ar^+ laser wavelength was less than 0.3 cm^{-1}. The major uncertainties in reported sample frequencies derive from changes in the dye laser wavelength due to temperature changes in the room. We expect the standard deviation of our frequency measurements to be within 0.3 cm^{-1}.

The gas-phase samples were prepared by introducing the NiOEP and CoOEP crystals into carefully cleaned 1.5-cm glass optical cells. These cells were evacuated to 10^{-3} torr on a vacuum line, sealed, and placed in a specially designed Raman oven that permitted 90° scattering. The oven was constructed with a temperature gradient of ca. 10 °C so that the cell front window was 10 °C hotter than the back. This prevented condensation of the gas-phase porphyrin on the optical window. We estimate that the temperature measurement error for the gas-phase samples is within ±20 °C.

The condensed-phase elevated-temperature NiOEP studies were obtained by using a rotating capillary cell in a resistively heated aluminum block. Crystals of NiOEP were dissolved in diffusion oil and introduced into capillaries that were degassed on a vacuum line and sealed. One end of the capillary was attached to a motor and placed in the oven and spun during the measurement. We estimate the likely temperature error for the diffusion-oil studies was within ±10 °C.

The low-temperature diffusion-oil measurements were obtained by using a specially designed cylindrical dewar. The 1.5 mm ID sample capillaries attached to a motor were spun within the cylindrical, transparent dewar. For temperatures above 77 K, cold nitrogen was flowed past the capillary, and the temperature was actively controlled by using a resistive heating element that heated the gas to the required temperature before it passed over the sample. Temperatures below 77 K were obtained by flowing cold helium past the sample.

(14) Marks, S.; Cornelius, P. A.; Harris, C. B. *J. Chem. Phys.* **1980**, *73*, 3068.
(15) Adler, A. D.; Longo, F. R.; Kampas, F.; Kim, J. *J. Inorg. Nucl. Chem.* **1970**, *32*, 2443.
(16) Bonnett, R.; Dimsdale, M. J. *J. Chem. Soc. Perkins Trans.* **1972**, 2540.
(17) Ogoshi, H.; Saito, Y.; Nakamoto, K. *J. Chem. Phys.* **1972**, *57*, 4194.
(18) Ogoshi, H.; Masai, N.; Yoshida, Z.; Takemoto, J.; Nakamoto, K. *Bull. Chem. Soc. Jpn.* **1971**, *44*, 49.
(19) Saitoh, K.; Koboyashi, M.; Suzuki, N. *Anal. Chem.* **1981**, *53*, 2309.
(20) Hui, K. S.; Davis, B. A.; Boulton, A. A. *J. Chromatogr.* **1975**, *115*, 581.
(21) Saitoh, K.; Kobayashi, M.; Suzuki, N. *J. Chromatogr.* **1982**, *243*, 291.
(22) Fuhrhop, J. H.; Mauzerall, D. *J. Am. Chem. Soc.* **1969**, *91*, 4174.

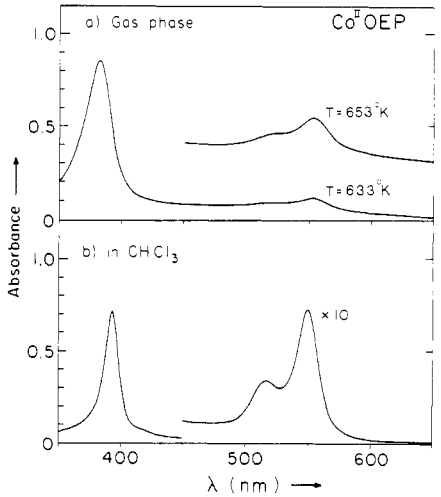

Figure 3. Absorption spectrum of cobalt(II) octaethylporphine: (a) in the gas phase at 653 and 633 K, path length = 1.5 cm; (b) in $CHCl_3$ solution at room temperature, path length = 1.0 cm, concentration $\simeq 2.9 \times 10^{-6}$ M.

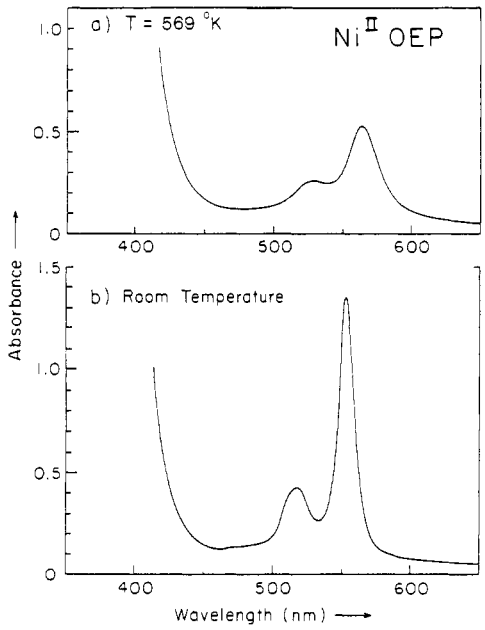

Figure 4. Absorption spectrum of nickel(II) octaethylporphine in silicone oil, path length $\simeq$ 0.1 cm, concentration $\simeq 3.5 \times 10^{-5}$ M: (a) at 569 K; (b) at room temperature.

During resonance Raman excitation, absorption of the beam by the sample causes local heating that results in an increased temperature within the scattering volume of the sample. We have examined this phenomenon both theoretically and experimentally, and these results will be reported in detail elsewhere.[23] However, for the low-temperature measurements in the frozen silicone oil the local temperature increase is less than 20 K. A smaller temperature increase occurs for the higher-temperature diffusion-oil measurements because of the thermal convection present in the liquid samples.

Results

Figures 2a and 3a show the absorption spectra of NiOEP and CoOEP in the gas phase at 630–660 K while Figures 2b and 3b show the absorption spectra of the same complexes in chloroform at room temperature. Figure 4 shows the absorption spectrum of NiOEP in diffusion oil at 569 K (Figure 4a) and at room temperature (Figure 4b). All of the absorption spectra show the characteristic porphyrin in-plane $\pi \rightarrow \pi^*$ electronic transitions. The intense Soret absorption band occurs at ca. 400 nm for all of these complexes while the two features at ca. 550 and 520 nm correspond to the α and β absorption bands, respectively. These absorption spectra are similar to gas-phase absorption measurements obtained earlier by Gouterman et al.[24,25] Shifts of ca. 10 nm to the blue occur for the Soret band of both NiOEP and CoOEP in the gas-phase samples compared to the room-temperature $CHCl_3$ solution samples (Table I). In contrast the α and β bands shift to the red by about 4 and 8 nm, respectively. The peaks in the gas-phase absorption spectra are also broadened compared to the spectra in $CHCl_3$ at room temperature.

To distinguish spectral changes which derive from the phase change from gas to solution from spectral changes which derive from the temperature increase, the absorption spectra of NiOEP dissolved in silicone oil were measured at room temperature and at 569 K. The shift to longer wavelength of the α and β bands in the high-temperature diffusion-oil spectrum from that observed at room temperature suggests that the increased temperature and not the phase change is primarily responsible for the absorption spectral differences between the gas-phase and the condensed-phase samples.

Although the similarities between the gas-phase and condensed-phase absorption spectra are a strong indication that no thermal decomposition of the metalloporphyrins occurred, we measured the mass spectra of a series of metalloporphyrins at low electron-impact energies. The porphyrins were introduced into the ionization chamber by heating the samples to 130 °C on a mass spectrometer solids probe. Figure 5a, which shows the mass spectrum of CoOEP, indicates the almost exclusive presence of the intact CoOEP parent ion with a mass of 591 amu. Similar results are obtained from NiOEP.

Other porphyrin complexes such as Fe^{III}OEPCl introduced into the gas phase display significantly different absorption spectra from that observed in $CHCl_3$ solution (Figure 6). A comparison of the gas-phase absorption spectrum of iron(III) etioporphin I chloride (Fe^{III}ETPCl) with those of Fe^{II}ETP(pyr)$_2$ and Fe^{III}ETPCl in solution suggests that the gas-phase species exists in the Fe(II)

Table I. Nickel(II) and Cobalt(II) Octaethylporphine Absorption Spectral Data

NiOEP				CoOEP			
$CHCl_3$ solution		gas phase		$CHCl_3$ solution		gas phase	
λ_{max}	fwhm[a]	λ_{max}	fwhm[a]	λ_{max}	fwhm[a]	λ_{max}	fwhm[a]
394	17	384	23	394	14	382	24
517	26	526		517		523	
553	17	557	23	552	24	557	45

[a] Full width at half maximum absorption.

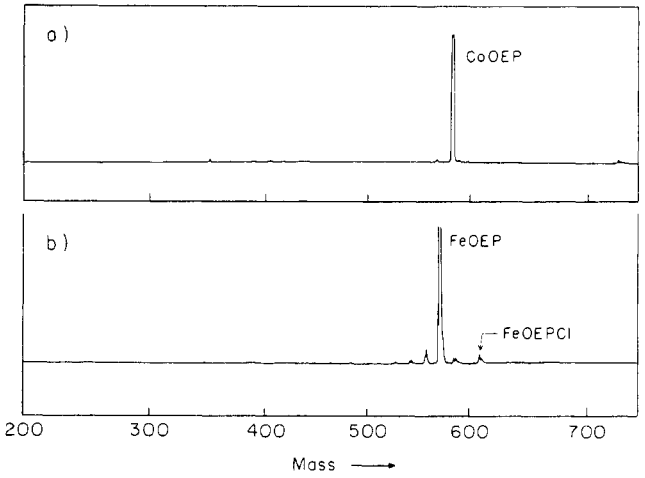

Figure 5. Mass spectrum (a) cobalt(II) octaethylporphine and (b) iron(III) octaethylporphine chloride. Electron impact energy = 15 eV.

(23) Asher, S. A.; Murtaugh, J.; Weber, S. G. *Appl. Spectrosc.*, submitted.

(24) Edwards, L.; Dolphin, D.; Gouterman, M. *J. Mol. Spectrosc.* **1970**, *35*, 90.

(25) Gouterman, M. "The Porphyrins"; Dolphin, D. Ed.; Academic Press: New York, 1978; Vol. III, Part A, pp 1–156.

Table II. Gas and Solution Raman Spectral Frequency Differences[a]

CoOEP			NiOEP				
gas 649 K	$CHCl_3$ soln 298 K	Δ	gas 653 K	$CHCl_3$ soln 298 K	Δ	band	% PED
1643	1653	−10	1640	1655	−15	ν_{10}	νC_aC_m (49), νC_aC_b (17)
1597	1603	−6	1588	1602	−14	ν_{19}	$\nu' C_aC_m$ (67), νC_aC_b (18)
~1569	~1578	~−10	1561	1576	−15	ν_{11}	$\nu' C_bC_b$ (57), $\nu C_{b\text{-}Et}$ (16)
1513	1517	−4				ν_3	νC_aC_m (41), νC_aC_b (35)
1320	1313	+7	1309	1308	+1	ν_{21}	$\delta' C_mH$ (53), $\nu' C_aC_b$ (18)
1222	1223	−1	1215	1219	−4	ν_{13}	δC_mH (67), νC_aC_b (22)
1164	1162	+2					
1029	1028	+1	1023	1023	0	ν_5	$\nu C_{b\text{-}Et}$ (38), νC_aC_b (23)
754			750	750	0	ν_{16}	δC_aNC_a (14), $\nu C_{b\text{-}Et}$ (15)

[a] Band numbering and PED contribution taken from Abe et al.[28] The potential energy distribution (PED) is one measure of the relative contribution of stretching (ν) and deformations (δ) of the α (C_a), β (C_b), and methine (C) carbon atoms of the porphyrin ring to the vibrational mode. Another measure is the magnitude of the atomic displacements that are pictorially illustrated in Abe et al.

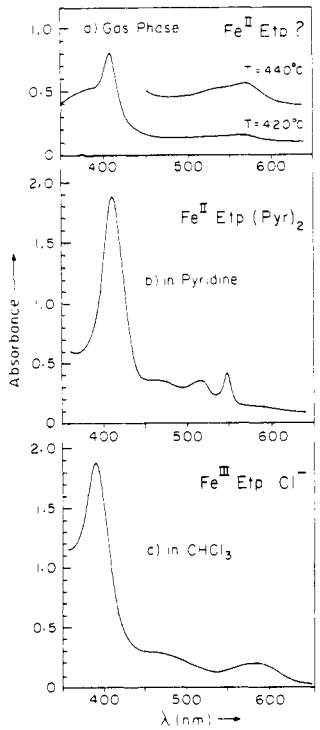

Figure 6. Absorption spectra (a) iron(III) etioporphine chloride in the gas phase, (b) the dipyridine complex of iron(II) etioporphrin in solution, at room temperature, and (c) iron(III) etioporphine chloride in $CHCl_3$ at room temperature.

oxidation state because of the similarity of the gas-phase spectrum to that of the $Fe^{II}ETP(pyr)_2$ complex. The mass spectral data shown in Figure 5b also indicate that the predominant species in the gas phase is a four-coordinate iron porphyrin, in agreement with previous reports;[24-27] only a small spectral feature exists in the mass spectrum corresponding to the parent $Fe^{III}OEPCl$ complex.

A comparison between the resonance Raman spectra of the gas- and condensed-phase porphyrin species excited at an identical wavelength at the α band absorption spectral maximum indicates that frequency differences occur for many of the Raman peaks. For example, a comparison of the gas-phase and room-temperature $CHCl_3$-solution resonance Raman spectra of NiOEP (Figure 7a,b) indicates that a general decrease in the Raman frequencies occurs for the gas-phase spectra compared to that of the room-temperature spectra. The difference spectrum in Figure 7c graphically illustrate these frequency shifts, and the data are tabulated in Table II. The porphyrin Raman peaks are labeled in Table II and in this text by using a numbering scheme devised by Abe et al.[28]

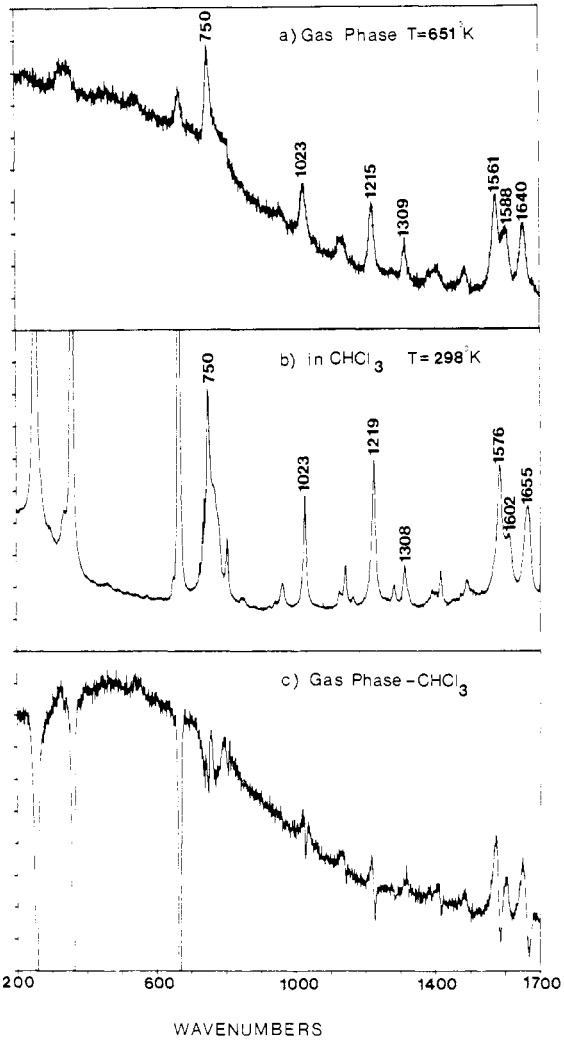

Figure 7. Resonance Raman spectra of nickel(II) octaethylporphine (a) in the gas phase, T = 651 K, λ_{ex} = 5565 Å, laser power = 0.5 W, band-pass ≃ 4 cm^{-1}, counting time = 1 s, scans = 2; (b) in $CHCl_3$ solution at room temperature, λ_{ex} = 5564 Å, laser power = 0.2 W, band-pass ≃ 4 cm^{-1}, counting time = 1 s, scans = 1; and (c) as a difference spectrum (spectrum a − spectrum b), peaks below 700 cm^{-1} in parts b and c which are off scale derive from the solvent $CHCl_3$.

Also included in Table II is a listing of the atoms involved in the nuclear displacements for each vibrational mode.

The structure-sensitive Raman peaks at ca. 1576, 1602, and 1655 cm^{-1} at room temperature which are known to be especially sensitive to alterations in the distance between the center of the heme core and the pyrrole nitrogen atoms ($R_{C_t\text{-}N}$)[29-32] show the

(26) Edwards, L.; Dolphin, D. H.; Gouterman, M.; Adler, A. D. *J. Mol. Spectrosc.* **1971**, *38*, 16.
(27) Edwards, L.; Gouterman, M. *J. Mol. Spectrosc.* **1970**, *33*, 292.
(28) Abe, M.; Kitagawa, T.; Kyogoku, Y. *J. Chem. Phys.* **1978**, *69*, 4526.

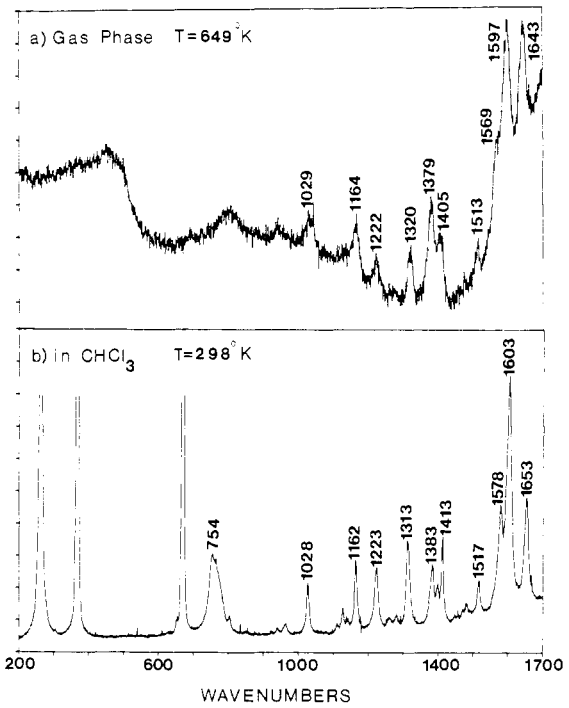

Figure 8. Resonance Raman spectra of cobalt(II) octaethylporphine: (a) in the gas phase, T = 649 K, λ_{ex} = 5145 Å, laser power = 1.2 W, band-pass $\simeq$ 4 cm^{-1}, counting time = 1 s, scans = 2; (b) in $CHCl_3$ at room temperature, λ_{ex} = 5145 Å, laser power = 0.5 W, band-pass $\simeq$ 4 cm^{-1}, counting time = 1 s, scans = 1.

largest frequency shifts in Figure 7 and are ca. 15 cm^{-1} lower in the high-temperature gas-phase spectra than in the $CHCl_3$-solution spectra. If the correlation between frequency and heme core size remains valid for the gas-phase porphyrins, then the data suggest that the heme core has expanded by ca. 0.03 Å. Other Raman peaks show smaller shifts. For example, the 750- and 1023-cm^{-1} peaks show little or no shifts in frequency, but each peak displays significant broadening in the Raman difference spectrum.

Resonance Raman spectra of gas-phase and room-temperature $CHCl_3$ solutions of CoOEP show similar differences (Figure 8); the peaks between 1550 and 1700 cm^{-1} shift down by ca. 10 cm^{-1} in the gas phase, while the 1028-cm^{-1} peak shows little or no frequency shift. Although the spectral shifts are similar in direction between NiOEP and CoOEP, the magnitudes of the shifts quantitatively differ. The data in Figures 7 and 8 were obtained by using a slit photomultiplier detector, and the expected precision in the frequencies listed is ±2 cm^{-1}.

An examination of nuclear vibrations involved in the normal mode can quantitatively rationalize the relative frequency shifts observed between the gas-phase and condensed-phase porphyrins. The Raman peaks containing large contributions of stretching and deformation about the C_a–C_m–C_a bonds such as the 1655- (ν_{10}), 1602- (ν_{19}), and 1576- (ν_{11}) cm^{-1} peaks show the largest shifts, while those vibrations containing large contributions of peripheral substituent stretches and deformations and methine hydrogen deformations such as the 750 cm^{-1} (ν_{16}) and 1023 cm^{-1} (ν_5) vibrations show only small frequency shifts.

To separate the contributions to the Raman frequency shifts of the phase change and the temperature difference occurring between the room-temperature $CHCl_3$-solution spectra and the high-temperature gas-phase spectra we determined the temperature dependence of the resonance Raman frequencies of NiOEP

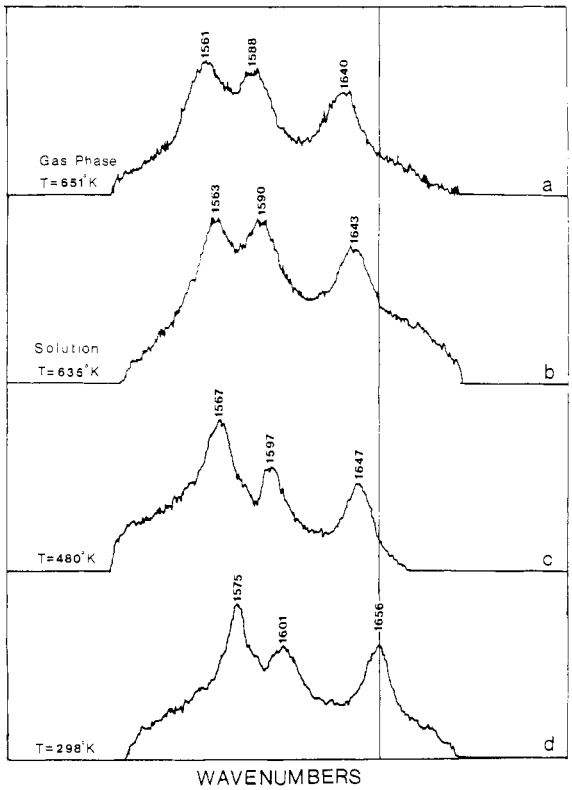

Figure 9. Resonance Raman spectra of nickel(II) octaethylporphine at band-pass $\simeq$ 4 cm^{-1}: (a) in the gas phase, T = 651 K, λ_{ex} = 5543 Å, laser power = 0.25 W; (b–d) in diffusion oil at the temperature indicated in the figure, λ_{ex} = 5544 Å, laser power = 0.03 W for b and 0.1 W for c and d. The contribution of diffusion oil to the Raman spectra was subtracted out of spectra b, c, and d by numerically subtracting diffusion-oil spectra obtained at each of the individual temperatures.

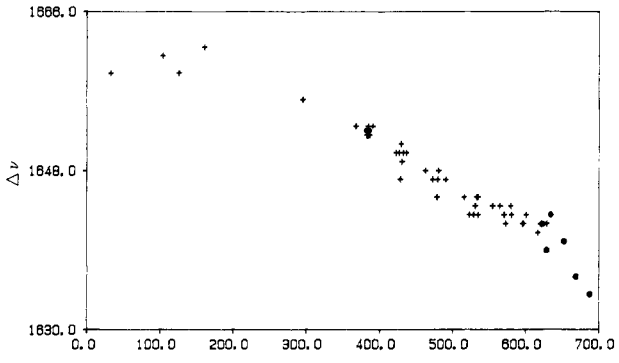

Figure 10. Temperature dependence of the ν_{10} vibrational frequency of Nickel(II) octaethylporphine. The crosses label frequencies of ν_{10} in diffusion-oil solutions of NiOEP, while the circles label the frequencies in the gas-phase samples.

dissolved in diffusion oil. Figure 9 shows the 1500–1700-cm^{-1} region of the Raman spectra of NiOEP dissolved in diffusion oil at 298, 480, and 635 K. Also shown in the gas-phase spectrum at 651 K. As indicated in the figure the frequencies of the Raman peaks decrease as the diffusion oil solution temperature increases. A small broadening also occurs for the NiOEP Raman peaks as the temperature increases. The similarity in peak widths for the 635 K diffusion-oil spectrum and the 651 K gas-phase Raman spectrum suggests that the Raman peak width derives from homogeneous broadening mechanisms.

The frequencies of the Raman peaks continually decrease as the temperature increases. Although NiOEP is known to adopt two different geometric forms in crystals,[29,33,34] and these forms

(29) Spaulding, L. D.; Chang, C. C.; Yu, N. T.; Felton, R. H. *J. Am. Chem. Soc.* **1975**, *97*, 2517.
(30) Huong, P. V.; Pommier, J.-C. *C. R. Hebd. Seances Acad. Sci., Ser. C* **1977**, *285*, 519.
(31) Spiro, T. G.; Stong, J. D.; Stein, P. *J. Am. Chem. Soc.* **1979**, *101*, 2648.
(32) Choi, S.; Spiro, T. G.; Langry, K. C.; Smith, K. M.; Budd, D. L.; LaMar, G. N. *J. Am. Chem. Soc.* **1982**, *104*, 4345.
(33) Scheuermann, W.; Nakamoto, K. *J. Mol. Struct.* **1978**, *48*, 285.

show different Raman frequencies, no evidence for different thermally populated geometric forms exists in the Raman spectra. The peak frequencies shift continuously with temperature and never display isosbestic points. Since the absorption spectra broaden and shift with increasing temperature, and the excitation wavelength is constant, it is possible that we are enhancing different thermally excited populations of NiOEP at the different temperatures. This is clearly not the case since shifts of the Raman frequencies in the high-temperature silicone-oil solutions do not occur if the excitation wavelength is altered.

Figure 10 shows the temperature dependence of the frequency of the ca. 1650-cm^{-1} ν_{10} vibration between 40 and 700 K. Both the diffusion-oil and the gas-phase data are shown. As indicated in Figure 10 a continuous decrease in frequency occurs for both the solution and gas-phase samples as the temperature increases. Indeed the magnitude of the frequency shift and the slope of the temperature dependence are almost identical for the gas and solution phases. These results indicate that little or no frequency difference exists between the gas and solution phases of NiOEP when both are measured at the same temperature; the frequencies of the porphyrin vibrations are apparently insensitive to the van der Waals interactions that occur in the condensed-phase solution samples of NiOEP.

Discussion

The large temperature dependence observed for the porphyrin ν_{10} vibration suggests that the heme core radius expands with temperature. This phenomenon probably occurs due to anharmonicities present in the thermally populated excited levels of low-frequency vibrations. As the low-frequency vibrations are thermally populated, their anharmonicity increases the porphyrin ring size. The high-frequency vibrations have previously been shown to systematically decrease in frequency as the distance between the pyrrole nitrogens and the center of the heme, R_{CtN}, increases. Presumably this derives from an expansion of the methine bridge angles which lead to a reduced force constant for the vibrations. Extensive empirical studies have demonstrated a nearly linear dependence of the frequency with the R_{CtN} distance.[29-32] Thus, $\nu = K(A - R_{CtN})$ where K and A are 517 cm^{-1}/Å and 5.16 Å, respectively, for the ν_{10} vibration. From the temperature-dependent data which are approximately linear between 250 and 500 K, one can propose a linear relationship between the R_{Ct-N} distance and the temperature

$$R_{CtN} = G(T - T_0) + V$$

where the parameter V derives from the R_{Ct-N} distance at 250 K, and G is the ratio of the slope of the temperature dependence of the frequency (−0.056 ± 0.006 cm^{-1}/°K) divided by the slope of the R_{Ct-N} frequency dependence, K. T_0 = 250 K. This empirical relationship should be approximately valid for temperatures between 250 and 500 K. The parameters G and V are found from our experimental data to be 1.1 × 10^{-4} Å/°K and 1.95 Å, respectively.

Porphyrins have numerous low-frequency vibrations that could contribute to the temperature-dependent frequency shifts. However, it is likely that some selectivity exists for particular vibrational modes that can expand the heme core. For example, anharmonicities present in vibrations of the pyrrole nitrogens against the metal or vibrations of the metal out of the heme plane are likely choices for vibrational modes that expand the R_{Ct-N} distance through anharmonicities.

Temperature Dependence of Vibrational Frequencies. Recent theoretical and experimental studies have examined the effect of temperature on vibrational frequencies and line shapes of polyatomic molecules. These studies have demonstrated that anharmonicities present in thermally populated low-frequency vibrations can effect the line widths and frequencies of higher-frequency vibrational fundamentals.[12-14] One model[12-14] consistent with our experimental data is illustrated in Figure 11. This model assumes a dynamic picture in which anharmonic coupling occurs

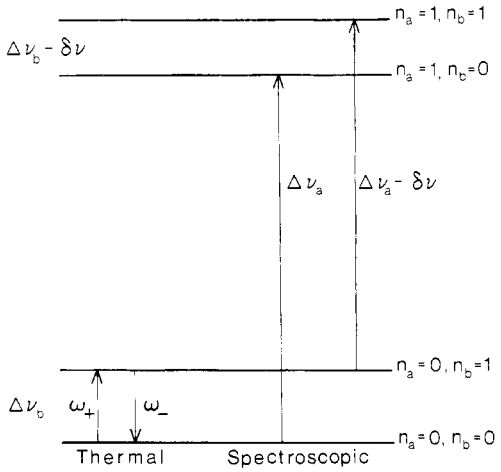

Figure 11. The spectroscopically observed fundamental vibration ν_a shows a frequency $\Delta\nu_a$ when the low-frequency vibration ν_b is in its ground state. Because of anharmonic coupling of ν_a and ν_b the frequency of $\Delta\nu_a$ is changed to $\Delta\nu_a - \delta\bar{\nu}$ as ν_b is thermally populated. n_a and n_b label the quanta of excitation in ν_a and ν_b, respectively.

between a vibrational mode ν_a which is monitored spectroscopically and a low-frequency mode ν_b which is thermally populated at the temperature of the spectral measurement and exchanges energy with other degrees of freedom in the molecule.

Because of anharmonic coupling of ν_a with ν_b, the frequency of the fundamental transition ν_a depends upon whether ν_b is thermally excited. The fundamental-transition frequency differs by the amount $\delta\nu$ depending on whether ν_b is thermally occupied. $\delta\nu$ may be either positive or negative, depending upon the value of cross terms in the anharmonic vibrational potential function. The exchange of energy in ν_b with other degrees of freedom of the molecule and in the environment modulates the frequency of ν_a. This leads to a temperature-dependent frequency and line width. The frequency is expected to show an exponential dependence on temperature,

$$\Delta\nu_a = \Delta\nu_0 + M \exp\frac{-hc\Delta\nu_b}{kT} \quad (1)$$

$$\Gamma = \Gamma_0 + D \exp\frac{-hc\Delta\nu_b}{kT} \quad (2)$$

where $\Delta\nu_a$ is the observed frequency of ν_a, T is the temperature, $\Delta\nu_0$ is the frequency at T = 0 K, $\Delta\nu_b$ is the frequency of the anharmonically coupled low-frequency mode, c is the speed of light, k is Boltzman's constant, and h is Planck's constant.

$$M = \frac{\delta\nu}{1 + (\delta\nu)^2\tau^2} \quad (3)$$

where $\delta\nu$ is the frequency difference for ν_a in the presence and absence of excitation in ν_b, and τ is the lifetime of the thermal excitation in mode ν_b. Deexcitation of mode ν_b can occur by either intramolecular energy exchange with other low-frequency vibrations which are of similar energy or intermolecular energy exchange with the surrounding bath. Γ is the line width, while Γ_0 is the line width at T = 0 K.

$$D = \frac{(\delta\nu)^2\tau}{1 + (\delta\nu)^2\tau^2} \quad (4)$$

These expressions for the vibrational frequency and line width predict an activation energy for the broadening and frequency shifts of peaks in the Raman spectra. Figure 12 shows the data from Figure 10 plotted as ln $(\Delta\nu_0 - \Delta\nu_a)$ vs. $1/T$. $\Delta\nu_0$ is the frequency at 0 K which is extrapolated from the data in Figure 10 to be 1662 cm^{-1}. It can be seen from Figure 12 that ln $(\Delta\nu_0 - \Delta\nu_a)$ is linear with respect to $1/T$. By recasting eq 1 as

$$\ln(\Delta\nu_0 - \Delta\nu_a) = \frac{-hc\Delta\nu_b}{k}\frac{1}{T} + \ln(-M) \quad (5)$$

(34) Cullen, D. L.; Meyer, E. F. *J. Am. Chem. Soc.* **1974**, *96*, 2095.

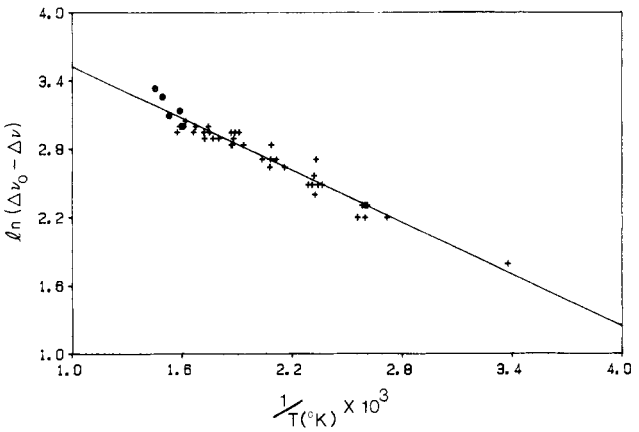

Figure 12. Temperature dependence of the ν_{10} vibrational frequency. The data derive from those data in Figure 10 but are plotted in terms of ln ($\Delta\nu_0 - \Delta\nu_a$) vs. $1/T$. $\Delta\nu_0$ is the extrapolated frequency at $T = 0$ K, $\Delta\nu_0 = 1662$ cm^{-1}.

one can calculate the effective activation energy for the temperature-dependent frequency shift of the ν_a vibration. We interpret this activation energy to derive from either one anharmonically active low-frequency vibration or from the contribution of a number of low-frequency vibrations. The calculated frequency of the vibrational mode ν_b responsible for the energy exchange and dephasing of the vibrational mode ν_{10} is 528 ± 150 cm^{-1}. Numerous low-frequency porphyrin vibrations occur below 500 cm^{-1}. Many of these are out-of-plane porphyrin vibrations or contain large contributions of pyrrole nitrogen–metal stretches.

The data do not permit a similar analysis for the line widths of the Raman peaks. The 1656-cm^{-1} peak in the 298 K sample shown in Figure 9 is assymetric and suggests a low-frequency shoulder at ca. 1635 cm^{-1}. This shoulder is clearly evident in the low-temperature 77 K spectrum (not shown). Because of the small intensity of this peak it does not interfere with measurements of the ν_{10} frequency. However, it prevents an accurate determination of the small changes in Raman line width that occur as the temperature increases.

Relevance to Transient Raman Studies. The data presented clearly indicate a large temperature dependence for the frequencies of those vibrational modes most characterized and useful for studying porphyrin geometric structure. Thus, caution is warranted if these vibrational frequencies are used for structural interpretations of resonance Raman heme protein frequency shifts if the heme temperature is changing. This represents a potential problem for transient resonance Raman studies of the photochemically generated transient species. For example, numerous studies have used photolysis in carbonmonoxy hemoglobin (HbCO) to generate a transient ferrous low-spin five-coordinated complex.[5-11] A subsequent probe pulse examines the Raman frequencies in order to monitor changes in geometry that occur as the heme relaxes to the high-spin ferrous five-coordinated form.

Since the photon energy used to generate the transient is significantly greater than the energy required to break the Fe–CO bond, net energy is deposited in the transient "deoxy heme". The heme is left in either an electronically or vibrationally excited state. Intramolecular relaxation occurs first to thermalize this energy in the ground-state electronic manifold to leave the heme at an elevated temperature. The heme will achieve thermal equilibrium with its surroundings during subsequent intermolecular relaxation. From the temperature-dependent frequency shifts observed for NiOEP and CoOEP one expects transient Raman frequency shifts to occur due to a transient heme temperature increase. The magnitude and temporal behavior of these frequency shifts can be estimated from previous data.

Bücher et al.[35] demonstrated that the HbCO photolysis quantum yield was independent of excitation wavelength from the UV spectral region to 546 nm, the longest wavelength used in their study. Further, Keyes et al.[36] in their equilibrium thermodynamic study of CO binding in myoglobin (Mb) determined that the ΔH for binding was ca. −22 kcal/mol for Sperm Whale Mb. The excess energy deposited in the heme and the CO ligand during photolysis can be estimated by considering the following cycle which models photolysis as a stepwise process in which a photon of energy $h\nu$ photolyzes HbCO to prepare Hb* and CO*$_{heme}$.

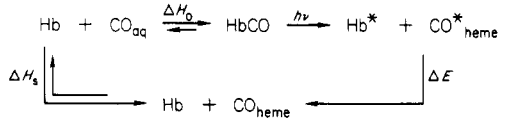

The superscript asterisk indicates that the CO and heme are in some excited state. CO_{heme} indicates a CO ligand localized somewhere within the heme crevice. Relaxation of the excited heme and CO ligand to thermal equilibrium with its surroundings deposits an energy ΔE into the globin and the solution, with the relaxed CO ligand remaining within the heme crevice. The last equilibrium step, exchange of CO between the heme crevice and the aqueous phase (CO_{aq}), has a heat of solution ΔH_s associated with it. ΔH_0, the experimentally observed enthalpy of ligand binding, incorporates ΔH_s for CO exchange between the heme crevice and the aqueous surroundings. The excess energy left in the heme and the CO ligand immediately after photolysis is $\Delta E = h\nu - h\nu_0$ where $h\nu_0$ is the minimum photon energy required for the photolysis reaction to occur. Thus,

$$\Delta E = \Delta H_s - H_0 - h\nu$$

If we model the heme crevice as a hydrophobic solvent, ΔH_s can be determined from the heat of solution difference between CO dissolved in water or benzene or some other hydrocarbon solvent.[37] ΔH_s can be calculated from the temperature dependence of the solubility of CO in water and in organic solvents and yields ΔH_s + 3 kcal/mol. For a photolysis excitation wavelength of 576 nm, which is the longest wavelength used in previously reported HbCO transient Raman studies,[7] $h\nu = 49.7$ kcal/mol. Thus, $\Delta E = 24.7$ kcal/mol is the excess energy remaining in the heme and free CO ligand after photolysis. Because the heme has a larger number of degrees of freedom than the CO almost all of this excess energy will remain localized in the heme.

Assuming a specific heat of 0.5 cal/°K g for the heme, one calculates a temperature increase for the heme of $\Delta T = 90$ °C. This temperature increase will result in a frequency decrease of ca. 5 cm^{-1} for the ν_{10}, ν_{19}, and ν_{11} heme Raman peaks. Whether this shift would be observed in the picosecond (ca. 25 ps) transient Raman studies will depend, of course, upon the relaxation rate of this energy out of the heme to the globin and surrounding solution. Direct information on the rate of thermal diffusion from the heme is not available. However, a number of recent studies have probed *intramolecular* vibrational relaxation rates. The intramolecular relaxation rate must represent a lower bound for the time constant of *intermolecular* relaxation and may underestimate it by a large factor. A variety of relaxation times are observed, all in the multipicosecond regime. The T_1 rate appears to strongly depend upon Fermi resonance interactions, Coriolis coupling, and resonance energy transfer.[38] For example, a long 220-ps thermal relaxation rate was observed for van der Waal complexes of helium and I_2 during supersonic jet photodissociation studies.[39,40] In contrast, energy decay of C–H stretching modes of $CHCl_3$, CH_2Cl_2, CH_3COCH_3, and CH_3OH gave lifetimes

(35) Bücher, T.; Kaspers, J. *Biochem. Biophys. Acta* **1947**, *1*, 21.

(36) Keyes, M. H.; Falley, M.; Lumry, R. *J. Am. Chem. Soc.* **1971**, *93*, 2035.

(37) Stephen, H.; and Stephen, T., Eds. "Solubilities of Inorganic and Organic Compounds"; McMillan Co.: New York, 1963; Vol. 1, Part 2, p 1053.

(38) Maier, J. P.; Seilmeir, A.; Kaiser, W. *Chem. Phys. Lett.* **1980**, *70*, 591.

(39) Johnson, K. E.; Wharton, L.; Levy, D. H. *J. Chem. Phys.* **1978**, *69*, 2719.

(40) Kenny, J. E.; Johnson, K. E.; Sharfin, W.; Levy, D. H. *J. Chem. Phys.* **1980**, *72*, 1109.

between 1.5 and 65 ps.[41] Relaxation rates of C–H stretching vibrations in the 400 molecular weight coumarin aromatic dyes gave relaxation rates of ca. 7 ps.[38] From these data it is likely that intermolecular relaxation rates should be sufficiently slow that it is likely that picosecond transient Raman studies will observe "hot" hemes.

The magnitude and direction of the frequency shifts which have been observed in the transient Raman studies of HbCO and HbO_2 are consistent with this possibility. For example, photolysis of HbCO with 30-ps 576-nm light[7] results in a transient deoxy Hb species with its ν_{10}, ν_{19}, and ν_{11} bands shifted down in frequency by 3–4 cm^{-1} compared to those of deoxy Hb. Photolysis of HbO_2 with 530-nm excitation results in a transient photoproduct with its ν_{10}, ν_{19}, and ν_{11} peaks down shifted compared to those of normal deoxy Hb by 15, 6, and 11 cm^{-1}, respectively. This transient species[10] decays within ca. 50 ps to another species with frequencies similar to the picosecond transient observed for MbCO.

Nanosecond transient Raman studies also observe frequency shifts for the ν_{10}, ν_{19}, and ν_{11} vibrations. However, it appears unlikely that the origin of these transients derives from "hot hemes" since thermal relaxation should have already occurred. Although the frequency shifts observed in the nanosecond HbCO studies are in the same direction as those for the picosecond studies, the imprecision of the picosecond and nanosecond data do not permit a quantitative comparison between the frequency shifts in the different time regimes. Further, no data exist for the time evolution of the shifts between the picosecond transient and the nanosecond transient.

Other data consistent with a "hot" hemes contribution to spectroscopic changes in the picosecond time regime are the broadened picosecond Soret, α- and β-absorption bands observed immediately following HbCO and HbO_2 photolysis.[42] The broadening is similar in direction and magnitude to that observed by heating NiOEP or CoOEP. The fact that these absorption spectral transients are not observed in studies of low-temperature trapped HbCO photolysis intermediate under steady state illumination conditions[43] is consistent with the possibility that the picosecond absorption transients derive from a hot heme. A change in the contacts between the globin amino acids and the heme should change the thermal relaxation rate. Possibly the difference in globin–heme contacts in Mb over Hb result in a faster T_1 for Mb and thus accounts for the smaller transient Raman frequency shifts observed for MbCO compared to HbCO.[5]

The above data and discussions suggest that care must be exercised when assigning transient Raman and absorption spectral changes to specific changes in heme excited states or molecular geometry. However, even if the transient studies only measure the rate of heat diffusion from the heme, these data can give important information on heme–globin contacts and should represent a useful technique for studying heme–globin interactions.

The effect of laser thermal heating on Raman frequencies must be considered during resonance Raman measurements. In photochemically generated picosecond transient measurements the temperature is localized in the photolyzed species. In longer pulse length measurement (nanosecond to continuous wave) the temperature increases are associated with an increase in temperature of the illuminated sample volume. For CW static measurements in solution a focused 100-mW laser beam can result in temperature increases of greater than 100 K in the illuminated sample volume.[23] Spinning the sample cell spreads the laser power over a larger volume. This results in an effective increase in the sample heat capacity and a negligible temperature increase. In contrast, because the rate of heat diffusion is slow, nanosecond and microsecond pulsed measurements can result in sample temperatures which approach those of the static CW measurement. For example, assume a 10-mJ laser pulse is absorbed within a cylinder of solution of diameter 0.02 cm which is 0.1-cm high. If no heat diffusion occurred during the time of the laser pulse and all of the energy relaxation was nonradiative, the temperature increase would correspond to 80 K. Thus, the same net temperature increase could occur in a picosecond transient measurement where the photochemical process selectively localizes the excess photon energy in the transient molecular species, and in a longer excitation pulse measurement where the bulk sample temperature increases during the laser excitation pulse due to the long times associated with bulk sample heat diffusion.

Acknowledgment. We gratefully acknowledge Professor David Pratt for the loan of a flowing helium dewar for the low-temperature studies reported here. We gratefully acknowledge support for this study from NIH Grant 1R01 GM 30751-01. We also gratefully acknowledge starter grant support from the Health Research and Services Foundation, Pittsburgh, Pa., Cottrell Research Corporation, and BRSG Grant 2S07 RR 07084-016 awarded by the Biomedical Research Support Grant Program, Division of Research Resources, National Institutes of Health. Acknowledgment is also made to the donors of the Petroleum Research Fund, administered by the American Chemical Society, for a starter grant and the Provost fund of the University of Pittsburgh.

Registry No. CoOEP, 17632-19-8; NiOEP, 24803-99-4; Fe^{III}OEPCl, 28755-93-3; Fe^{III}EtPCl, 19413-49-1; $Fe^{II}EtP(pyr)_2$, 87761-64-6.

(41) Fendt, A.; Fischer, S. F.; Kaiser, W. *Chem. Phys.* **1981**, *57*, 55.
(42) Greene, B. I.; Hochstrasser, R. M.; Weisman, R. B.; Eaton, W. A. *Proc. Natl. Acad. Sci. U.S.A.* **1978**, *75*, 5255.
(43) Iizuka, T.; Yamamoto, H.; Kotani, M.; Yonetani, T. *Biochim. Biophys. Acta* **1974**, *371*, 126.